Shape Recovery of Deformed Biomolecular Droplets: Dependence on Condensate Viscoelasticity

Huan-Xiang Zhou*

Department of Chemistry and Department of Physics, University of Illinois at Chicago, Chicago, Illinois 60607, USA

*hzhou43@uic.edu

ABSTRACT

Phase-separated biomolecular condensates often appear as micron-sized droplets. Due to interfacial tension, the droplets usually have a spherical shape and, upon deformation, tend to recover their original shape. Likewise, interfacial tension drives the fusion of two droplets into a single spherical droplet. In all previous studies on shape dynamics, biomolecular condensates have been modeled as purely viscous. However, recent work has shown that biomolecular condensates are viscoelastic, with shear relaxation occurring not instantaneously as would in purely viscous fluids. Here we present an exact analytical solution for the shape recovery dynamics of biomolecular droplets, which exhibits rich time dependence due to viscoelasticity. For condensates modeled as purely viscous, shape recovery is an exponential function of time, with the time constant given by the "viscocapillary" ratio, i.e., viscosity over interfacial tension. For viscoelastic droplets, shape recovery becomes multi-exponential, with shear relaxation yielding additional time constants. The longest of these time constants can be dictated by shear relaxation and independent of interfacial tension, thereby challenging the currently prevailing viscocapillarity-centric view derived from purely viscous fluids. These results highlight the importance of viscoelasticity in condensate shape dynamics and expand our understanding of how material properties affect condensate dynamics in general, including aging. The analytical solution presented here can also be used for validating numerical solutions of fluid-dynamics problems and for fitting experimental and molecular simulation data.

Subject Areas: Biological Physics, Fluid Dynamics, Soft Matter

I. INTRODUCTION

Phase-separated biomolecular condensates exhibit different extents of liquidity, which may be crucial for cellular functions and correlated with diseases such as neurodegeneration and cancer [1-7]. Driven by interfacial tension (or capillarity), condensates that are more liquid-like retain a spherical shape and hence appear as micro-sized droplets. The material properties of many condensates also evolve over time and become more solid-like (sometimes referred to as "aging") [8-13]. A simple indication of liquidity is the tendency of deformed droplets to recover their spherical shape. In all the studies so far on the dynamics of such shape changes, biomolecular condensates have been modeled as purely viscous, reporting viscosities that are orders of magnitude higher than that of water [1,8,14-18]. However, recent work has shown that condensates are viscoelastic [12,19-21]. In viscoelastic fluids, shear relaxation is not instantaneous [21] and its effects, when coupled with viscocapillary effects, can lead to unexpected observations. In this work we present a theoretical study on the effects of viscoelasticity on the shape recovery dynamics of deformed biomolecular droplets.

Nearly all previous studies on the shape dynamics of biomolecular condensates have dealt with the fusion of droplets when they come into contact [1,8,11,14-18,22-26]. However, in one study, Hubstenberger et al. [1] reported observations on both droplet fusion and shape recovery, and found the latter to be fast by two orders of magnitude. These authors suggested that the disparity in timescales between the two kinds of shape dynamics indicated viscoelasticity. While theoretical results of viscous fluids have been used for qualitative as well as quantitative analysis of droplet fusion dynamics [1,14-18,26] and a theoretical model of viscoelastic fluids has been introduced to treat deformation of droplets under external force [19,20], up to now no theory has been presented for shape recovery of biomolecular droplets.

The disparity in timescales between droplet fusion and shape recovery has remained a mystery.

Shape recovery of deformed droplets has long received attention in the fluid-dynamics literature. Prosperetti [27,28] presented a full analytical solution to the recovery dynamics of viscous droplets from a small-amplitude deformation. Theoretical results for shape recovery, also known as deformation retraction, of viscoelastic droplets have also been presented, by approximating the deformed shape as an ellipsoid [29,30]. This problem has also been tackled by numerically solved the fluid-dynamics equations [31-33]. There have also been a number of experimental studies on the deformation retraction of polymer blends [34-37], often indicating the effects of viscoelasticity.

The high viscosities reported for biomolecular condensates (relative to water) translate into a significant viscosity ratio, $\eta_{\mathrm{II}}/\eta_{\mathrm{I}}$, between the dense droplet phase (indicated by index II; Fig. 1) and the exterior dilute bulk phase (indicated by index I) as found in *in vitro* studies. On the other hand, Caragine et al. [22] suggested a case with $\eta_{\mathrm{II}}/\eta_{\mathrm{I}} \ll 1$. They noted the even higher viscosity of the nucleoplasm surrounding nucleoli, a type of biomolecular condensates specializing in ribosomal biogenesis, than that of droplets formed by a main nucleolar protein [17]. In addition, polymer blends may phase separate to produce dilute-phase "bubbles" in dense coacervates [37], also leading to $\eta_{\mathrm{II}}/\eta_{\mathrm{I}} \ll 1$. The viscosity ratio is of theoretical interest because in the limiting cases of $\eta_{\mathrm{II}}/\eta_{\mathrm{I}} = \infty$ and 0 one can neglect the fluid dynamics in either the exterior region (i.e., "I") or interior region (i.e., "II"), significantly simplifying the mathematics. The viscosity ratio may also affect how viscoelasticity affects shape dynamics.

Here we develop an analytical solution for the shape recovery dynamics of deformed viscoelastic droplets. In Sec. II we summarize the solution of Prosperetti for viscous fluids

[27,28] and present a new solution that is amenable to generalization to viscoelastic fluids. The solution for viscoelastic fluids is then presented in Sec. III. In Sec. IV we present shape recovery curves for selected values of viscosities and shear relaxation rates, to illustrate rich effects of viscoelasticity. Concluding remarks are given in Sec. V. Four Appendices contain further details.

II. INTERFACE SHAPE RCOVERY: NEWTONIAN FLUIDS

Our main interest is biomolecular droplets formed by phase separation. Due to vast differences in macromolecular concentrations between the droplet phase and the surrounding bulk phase, the viscosity in the droplet phase is much higher than the counterpart in the bulk phase, i.e., $\eta_{\mathrm{II}} \gg \eta_{\mathrm{I}}$. Neglecting the viscosity of the bulk phase (i.e., approximating the latter as an ideal fluid) leads to significant simplification of the solution of the fluid-dynamics problem. We then denote the viscosity of the droplet phase as η, without the subscript "II".

For some polymer blends, phase separation leads to polymer-poor "bubbles" forming in the coacervate matrix [37]. In this case, $\eta_{\mathrm{I}} \gg \eta_{\mathrm{II}}$; we then neglect η_{II} and denote the viscosity of the coacervate phase as η, without the subscript "I". We only retain the subscripts I and II when considering the full problem where both interior and exterior fluid dynamics are treated.

A. Fluid-dynamics problem

The shape change of a liquid droplet inside an ideal-fluid medium is dictated by the interior fluid dynamics, which we model by the (generalized) Navier-Stokes equations. The

first of these equations expresses mass conservation, which for an incompressible fluid has the form

$$\nabla \cdot \mathbf{v}(\mathbf{x}, t) = 0, \tag{1}$$

where $\mathbf{v}(\mathbf{x}, t)$ is the fluid velocity at position $\mathbf{x}$ and time t. The second of the Navier-Stokes equations expresses momentum conservation,

$$\varrho \left(\frac{\partial \mathbf{v}}{\partial t} + \mathbf{v} \cdot \nabla \mathbf{v} \right) = \nabla \cdot \tilde{\tau}, \tag{2}$$

where ϱ is the fluid density and $\tilde{\tau}$ is the stress tensor. Closure of this equation requires a constitutive relation for $\tilde{\tau}$. One contribution to $\tilde{\tau}$ is hydrostatic pressure (p); the remaining contribution comes from fluid viscosity:

$$\tilde{\tau} = -p\tilde{I} + \tilde{\tau}_{\mathrm{d}}, \tag{3a}$$

where $\tilde{I}$ is the unit tensor. For purely viscous, or Newtonian fluids, the second contribution is given by

$$\tilde{\tau}_{\mathrm{d}} = \eta \tilde{\varepsilon}, \tag{3b}$$

where η is the fluid viscosity, and

$$\tilde{\varepsilon} = \nabla \mathbf{v} + (\nabla \mathbf{v})^{\mathrm{T}} \tag{3c}$$

is the symmetrized strain-rate tensor; the superscript "T" denotes transpose. The momentum equation then becomes

$$\varrho \left(\frac{\partial \mathbf{v}}{\partial t} + \mathbf{v} \cdot \nabla \mathbf{v} \right) = -\nabla p + \eta \nabla^2 \mathbf{v}. \tag{4a}$$

Biomolecular condensates have very high viscosity. Then the inertial terms on the left-hand-side of Eq. (4a) can be neglected, leading to

$$-\nabla p + \eta \nabla^2 \mathbf{v} \approx 0. \tag{4b}$$

The reduction of Eq. (4a) to Eq. (4b) is similar to the reduction, at high frictions, of the equation of motion for a Langevin particle to one representing Brownian dynamics.

To solve Eqs. (1) and (4a) [or (4b)], we have to specify boundary conditions. One is a "kinematic" boundary condition, which expresses the fact that fluid motions lead to changes in the shape of the interface between the droplet and bulk phases. If the interface at time t is specified by the condition

$$\mathcal{S}(\mathbf{x}, t) = 0, \qquad \text{when } \mathbf{x} \in \text{the interface}, \tag{5}$$

then the kinematic boundary condition is

$$\frac{\partial \mathcal{S}}{\partial t} + \mathbf{v} \cdot \nabla \mathcal{S} = 0. \tag{6}$$

The outward unit normal vector of the interface is given by

$$\mathbf{n} = \frac{\nabla \mathcal{S}}{|\nabla \mathcal{S}|}. \tag{7}$$

The remaining boundary conditions express force balance at the interface:

$$\mathbf{n} \cdot \tilde{\tau} \cdot \mathbf{t} = 0, \tag{8}$$

$$\mathbf{n} \cdot \tilde{\tau} \cdot \mathbf{n} = -\gamma \nabla \cdot \mathbf{n}, \qquad \text{for droplets}, \tag{9}$$

where $\mathbf{t}$ denotes a unit vector along a tangential direction of the interface, and γ is the interfacial tension. Note that, due to the much higher viscosity inside biomolecular droplets than in the surrounding bulk phase, the effect of the velocity field in the bulk phase has been neglected. A constant pressure in the bulk phase can be accounted for by subtracting it from the interior pressure. Therefore, the two force-balance boundary conditions involve only the interior stress tensor.

In the case of ideal-fluid bubbles in a Newtonian-fluid medium, the shape change is dictated by the exterior fluid dynamics. All but one of the above equations still hold when the

symbols denote exterior properties. The one exception is a sign change in the boundary condition of Eq. (9):

$$\mathbf{n} \cdot \tilde{\tau} \cdot \mathbf{n} = \gamma \nabla \cdot \mathbf{n}, \qquad \text{for bubbles.} \tag{10}$$

The problem at hand is to find the interface shape function $\mathcal{S}(\mathbf{x}, t)$ at any time t, given the initial shape function $\mathcal{S}(\mathbf{x}, 0)$ (and its initial rate $\left.\frac{\partial \mathcal{S}}{\partial t}\right|_{t=0}$ if necessary). Due to the interfacial tension, a deformed droplet will recover its spherical shape; we refer to this process shape recovery. Other terms used in the literature include deformation retraction or relaxation.

B. Solution of Prosperetti

Prosperetti [27] solved the shape recovery problem for small-amplitude deformation. That is, the initial shape of the interface bewteen a droplet and the bulk phase (approximated as ideal fluid) was assumed to be a small deformation from a sphere with radius R. Using spherical coordinates (r, θ, ϕ) for the position $\mathbf{x}$ (with origin at the center of the reference sphere), the radial distance of the interface at polar angle θ and azimuthal angle ϕ and at time t can be written as (Fig. 1)

$$r(\theta, \phi, t) = R + f_l(t) Y_{lm}(\theta, \phi), \tag{11}$$

where $Y_{lm}(\theta, \phi)$ is a spherical harmonic. Because of the orthogonality of sphercial harmonics, we can later add up the results for individual spherical harmonics to obtain a complete solution. The amplitude $f_l(t)$ satisfies the following integro-differential equation:

$$\ddot{f}_l(t) + b\dot{f}_l(t) - bc \int_0^t dt' Q(t - t')\, \dot{f}_l(t') + \varpi_0^2 f_l(t) = 0, \tag{12}$$

where dots denote differentiation with respect to time,

$$b = \frac{2(l-1)(2l+1)\eta}{\varrho R^2}, \tag{13a}$$

$$c = \frac{(l-1)(l+1)}{2l+1}, \tag{13b}$$

$$\varpi_0^2 = \frac{l(l-1)(l+2)\gamma}{\varrho R^3}, \tag{13c}$$

and for the function $Q(t)$ only its Laplace transform is known. Denoting the Laplace transform of any function of time, $g(t)$, as $\hat{g}(s)$, we have

$$\hat{Q}(s) = \frac{1}{\frac{wI_{l+1/2}(w)}{2I_{l+3/2}(w)} - 1} \equiv \frac{1}{\frac{1}{2}\mathcal{I}_l(w) - 1}, \tag{13d}$$

where $w = R\sqrt{\varrho s/\eta}$ and $I_{l+1/2}(x)$ are modified Bessel functions of the first kind.

Prosperetti [27] considered the long-time asymptotic behavior of $f_l(t)$, where $f_l(t) \approx C(t)e^{-\nu_l t}$ with $C(t)$ becoming a finite constant as $t \to \infty$, leading to an equation for ν_l that is identical to the classical result of Chandrasekhar [38] and Reid [39] using normal-mode analysis. This analysis has now been extended to viscoelastic droplets in an ideal fluid [40,41].

Here our concern is the initial value problem, i.e., the time dependence of $f_l(t)$ starting from $t = 0$. We are particularly interested in the high-friction regime. In this regime, we neglect the second derivative, $\ddot{f}_l(t)$, in Eq. (12), similar to reducing the Langevin equation to one representing Brownian dynamics. Furthermore, high friction means $w \to 0$ and hence we approximate $\hat{Q}(s)$ as

$$\hat{Q}(s) \approx \lim_{w\to 0} \hat{Q}(s) = \frac{2}{2l+1}. \tag{13e}$$

This result is independent of s, meaning that $Q(t)$ is a delta function of time. The solution of Eq. (12) is an exponential function,

$$f_l(t) = f_l(0)e^{-\lambda_l^{\mathrm{D}} t}, \tag{14}$$

with the recovering rate given by

$$\lambda_l^{\mathrm{D}} = \frac{l(l+2)(2l+1)}{2(2l^2+4l+3)}\frac{\gamma}{\eta R}. \tag{15}$$

For ideal-fluid bubbles, Eq. (12) still holds, but with

$$b = \frac{2(l+2)(2l+1)\eta}{\varrho R^2}, \tag{16a}$$

$$c = \frac{l(l+2)}{2l+1}, \tag{16b}$$

$$\varpi_0^2 = \frac{(l-1)(l+1)(l+2)\gamma}{\varrho R^3}, \tag{16c}$$

$$\hat{Q}(s) = \frac{1}{\dfrac{wK_{l+1/2}(w)}{2K_{l-1/2}(w)} + 1} \equiv \frac{1}{\dfrac{1}{2}\mathcal{K}_l(w) + 1}, \tag{16d}$$

where $K_{l+1/2}(x)$ are modified Bessel functions of the second kind. Again our interest is the high-friction regime, where $w \to 0$ and $\hat{Q}(s)$ of Eq. (16d) approaches the same limit as given by Eq. (13e). The solution for $f_l(t)$ remains an exponential function, with the recovery rate now given by

$$\lambda_l^{\mathrm{B}} = \frac{(l-1)(l+1)(2l+1)}{2(2l^2+1)}\frac{\gamma}{\eta R}. \tag{17}$$

Prosperetti [28] also solved the full problem where both interior and exterior fluid dynamcis are treated, i.e., without invoking $\eta_{\mathrm{II}} \gg \eta_{\mathrm{I}}$ or $\eta_{\mathrm{II}} \ll \eta_{\mathrm{I}}$. Equation (12) becomes

$$\ddot{f}_l(t) + d^{-1}\int_0^t dt'\mathfrak{Q}(t-t')\,\dot{f}_l(t') + \varpi_0^2 f_l(t) = 0, \tag{18}$$

where

$$d = [(l+1)\varrho_{\mathrm{II}} + l\varrho_{\mathrm{I}}]R^2, \tag{19a}$$

$$\varpi_0^2 = \frac{l(l-1)(l+1)(l+2)\gamma}{dR}, \tag{19b}$$

$$\widehat{\mathfrak{Q}}(s) = \frac{\left\{\begin{array}{c}[(2l+1)\eta_{\mathrm{II}}\mathcal{J}_l(w_{\mathrm{II}}) - 2l(l+2)(\eta_{\mathrm{II}} - \eta_{\mathrm{I}})] \\ \times [(2l+1)\eta_{\mathrm{I}}\mathcal{K}_l(w_{\mathrm{I}}) + 2(l-1)(l+1)(\eta_{\mathrm{II}} - \eta_{\mathrm{I}})]\end{array}\right\}}{\eta_{\mathrm{II}}\mathcal{J}_l(w_{\mathrm{II}}) + \eta_{\mathrm{I}}\mathcal{K}_l(w_{\mathrm{I}}) - 2(\eta_{\mathrm{II}} - \eta_{\mathrm{I}})}, \tag{19c}$$

with subscripts "II" and "I" denoting quanties in the interior and exterior of the droplet. In the high-friction regime,

$$\widehat{\mathfrak{Q}}(s) \approx \frac{[(2l^2+4l+3)\eta_{II} + 2l(l+2)\eta_I][2(l-1)(l+1)\eta_{II} + (2l^2+1)\eta_I]}{(2l+1)(\eta_{II}+\eta_I)}, \tag{19d}$$

and $f_l(t)$ is an exponential funciton of time, with the recovery rate given by

$$\lambda_l = \frac{e_l(\alpha_{\mathrm{II/I}}+1)}{(a_l\alpha_{\mathrm{II/I}} + b_l)(c_l\alpha_{\mathrm{II/I}} + d_l)}\frac{\gamma}{\eta_I R}, \tag{20a}$$

where

$$a_l = 2l^2 + 4l + 3, \tag{20b}$$

$$b_l = 2l(l+2), \tag{20c}$$

$$c_l = 2(l-1)(l+1), \tag{20d}$$

$$d_l = 2l^2 + 1, \tag{20e}$$

$$e_l = l(l-1)(l+1)(l+2)(2l+1), \tag{20f}$$

$$\alpha_{\mathrm{II/I}} = \frac{\eta_{II}}{\eta_I}. \tag{20g}$$

One can easily verify that λ_l reduces to λ_l^{D} when $\alpha_{\mathrm{II/I}} \gg 1$ and to λ_l^{B} when $\alpha_{\mathrm{II/I}} \ll 1$.

C. New Solution

Here present a new solution for the shape recovery dynamics in the high-friction regime. This solution easily lends itself to generalization from viscous fluids to viscoelastic

fluids. The derivation here for droplets largely follows the solution of a related fluid-dynamics problem [20]. We assume that the shape deformation is axisymmetric (Fig. 1). Equation (11) then reduces to

$$r(\theta, t) = R + f_l(t) P_l(\cos\theta), \tag{21}$$

where $P_l(x)$ is a Legendre polynomial. Note that the lowest l should be 2, since $l = 0$ corresponds to a change in droplet radius and thus a violation of volume conservation demanded by fluid incompressibility, and $l = 1$ corresponds to a translational motion of the entire interface. We will keep terms only up to the first order in $f_l(t)$; to this order, the volume of the droplet is a constant when $f_l(t)$ changes over time.

The interface shape function can be identified as

$$\mathcal{S}(\mathbf{x}, t) = r - [R + f_l(t) P_l(\cos\theta)]. \tag{22}$$

The outward normal vector of the interface [Eq. (7)] can be found as

$$\mathbf{n} = \mathbf{e}_r - f_l(t) \nabla P_l(\cos\theta) = \mathbf{e}_r - \frac{f_l(t)}{R} \frac{\partial P_l(\cos\theta)}{\partial\theta} \mathbf{e}_\theta \tag{23}$$

to the first order in $f_l(t)$. The divergence of $\mathbf{n}$ is

$$\begin{aligned} \nabla \cdot \mathbf{n} &= \frac{2}{R} - \frac{2}{R^2} f_l(t) P_l(\cos\theta) - \frac{f_l(t)}{R^2 \sin\theta} \frac{\partial}{\partial\theta}\left(\sin\theta \frac{\partial P_l(\cos\theta)}{\partial\theta}\right) \\ &= \frac{2}{R} + \frac{(l-1)(l+2)}{R^2} f_l(t) P_l(\cos\theta). \end{aligned} \tag{24}$$

The fluid velocity $\mathbf{v}(\mathbf{x}, t)$ is of the same order as $f_l(t)$. Similarly, the pressure should only deviate from the static pressure that balances the interfacial tension of a spherical droplet by an amount, $\delta p(\mathbf{x}, t)$, that is of the same order as $f_l(t)$:

$$p(\mathbf{x}, t) = \frac{2\gamma}{R} + \delta p(\mathbf{x}, t). \tag{25}$$

The kinematic boundary condition [Eq. (6)] yields

$$\dot{f}_l(t)P_l(\cos\theta) = v_r \text{ at } r = R. \tag{26}$$

Subscripts r and θ denote the components of the velocity. The force-balance boundary conditions [Eqs. (8) and (9)] lead to

$$\frac{\partial v_r}{\partial \theta} + r\frac{\partial v_\theta}{\partial r} - v_\theta = 0 \; at \; r = R, \tag{27}$$

$$-\delta p + 2\eta\frac{\partial v_r}{\partial r} = -\frac{\gamma}{R^2}(l-1)(l+2)f_l(t)P_l(\cos\theta) \text{ at } r = R. \tag{28}$$

The velocity and pressure fields for an axisymmetric problem can be expressed in terms of the stream function $\Psi(r,\theta,t)$. For the interior problem considered here for droplets, the stream function has the form [42]

$$\Psi = [A(t)r^{l+3} + B(t)r^{l+1}]Q_l(\cos\theta), \tag{29}$$

where $A(t)$ and $B(t)$ are coefficients to be determined by the boundary conditions, and $Q_l(x)$ are related to Legendre polynomials $P_l(x)$ via

$$Q_l(x) = \int_{-1}^{x} dx' \, P_l(x') = \frac{P_{l+1}(x) - P_{l-1}(x)}{2l+1}. \tag{30}$$

The components of the velocity and the pressure are given by

$$v_r = -\frac{1}{r^2}\frac{\partial \Psi}{\partial \cos\theta} = -[A(t)r^{l+1} + B(t)r^{l-1}]P_l(\cos\theta), \tag{31}$$

$$v_\theta = -\frac{1}{r\sin\theta}\frac{\partial \Psi}{\partial r} = -[A(t)(l+3)r^{l+1} + B(t)(l+1)r^{l-1}]\frac{Q_l(\cos\theta)}{\sin\theta}, \tag{32}$$

$$\frac{\delta p}{2\eta} = -A(t)\left(2 + \frac{3}{l}\right)r^l P_l(\cos\theta). \tag{33}$$

Substituting Eqs. (31) and (32) into Eq. (27) leads to

$$l(l+2)\bar{A}(t) + (l-1)(l+1)\bar{B}(t) = 0, \tag{34}$$

where $\bar{A}(t) = A(t)R^l$ and $\bar{B}(t) = B(t)R^{l-2}$. Similarly, using Eqs. (31) and (33) in Eq. (28) leads to

$$\frac{l^2 - l - 3}{l}\bar{A}(t) + (l-1)\bar{B}(t) = \frac{\gamma}{2\eta R^2}(l-1)(l+2)f_l(t). \tag{35}$$

The results for $\bar{A}(t)$ and $\bar{B}(t)$ are:

$$\bar{A}(t) = -\frac{l(l-1)(l+1)(l+2)}{2(2l^2+4l+3)}\frac{\gamma f_l(t)}{\eta R^2}, \tag{36a}$$

$$\bar{B}(t) = \frac{l^2(l+2)^2}{2(2l^2+4l+3)}\frac{\gamma f_l(t)}{\eta R^2}. \tag{36b}$$

When these last results are inserted into Eq. (31), we find

$$v_r(R,\theta,t) = -\lambda_l^{\mathrm{D}} f_l(t) P_l(\cos\theta), \tag{37}$$

where λ_l^{D} is given by Eq. (15). Substituting Eq. (37) in Eq. (26) yields

$$\dot{f}_l(t) + \lambda_l^{\mathrm{D}} f_l(t) = 0. \tag{38}$$

The solution of this last equation is the exponential function in Eq. (14).

In preparation for the generalization to viscoelastic fluids, let us solve the problem again, now using Laplace transforms. The governing equations (1) and (4b) and the force-balance boundary conditions [Eqs. (27) and (28)] have the same form in Laplace space as they have in the time domain, as does the general form of the stream function [Eq. (29)]. Therefore Eqs. (34) and (35) take the same form in Laplace space:

$$l(l+2)\hat{\bar{A}}(s) + (l-1)(l+1)\hat{\bar{B}}(s) = 0, \tag{39}$$

$$\frac{l^2 - l - 3}{l}\hat{\bar{A}}(s) + (l-1)\hat{\bar{B}}(s) = \frac{\gamma}{2\eta R^2}(l-1)(l+2)\hat{f}_l(s). \tag{40}$$

The kinematic boundary condition [Eq. (26)] now takes the form

$$[s\hat{f}_l(s) - f_l(0)]P_l(\cos\theta) = \hat{v}_r \text{ at } r = R. \tag{41a}$$

Using Eq. (31) in the preceding equation, we find

$$s\hat{f}_l(s) = f_l(0) - [\hat{\bar{A}}(s) + \hat{\bar{B}}(s)]R. \tag{41b}$$

Solving Eqs. (39), (40), and (41b), we find

$$\hat{\bar{A}}(s) = -\frac{\frac{\gamma}{R^2} l(l-1)(l+1)(l+2) f_l(0)}{2\eta s(2l^2+4l+3) + \frac{\gamma}{R} l(l+2)(2l+1)}, \tag{42a}$$

$$\hat{\bar{B}}(s) = \frac{\frac{\gamma}{R^2} l^2(l+2)^2 f_l(0)}{2s\eta(2l^2+4l+3) + \frac{\gamma}{R} l(l+2)(2l+1)}, \tag{42b}$$

$$\hat{f}_l(s) = \frac{2\eta(2l^2+4l+3) f_l(0)}{2s\eta(2l^2+4l+3) + \frac{\gamma}{R} l(l+2)(2l+1)} = \frac{f_l(0)}{s+\lambda_l^{\mathrm{D}}}. \tag{42c}$$

The inverse Laplace transform of the foregoing $\hat{f}_l(s)$ is given by Eq. (14).

For the exterior problem appropriate for bubbles, the stream function is [42]

$$\Psi = [C(t) r^{-l+2} + D(t) r^{-l}] Q_l(\cos\theta). \tag{43}$$

Analogous to Eqs. (31) – (33), we find the velocity and pressure to be

$$v_r = -[C(t) r^{-l} + D(t) r^{-l-2}] P_l(\cos\theta), \tag{44}$$

$$v_\theta = [(l-2) C(t) r^{-l} + l D(t) r^{-l-2}] \frac{Q_l(\cos\theta)}{\sin\theta}, \tag{45}$$

$$\frac{p}{2\eta} = -\frac{\gamma}{\eta R} - \frac{2l-1}{l+1} C(t) r^{-l-1} P_l(\cos\theta). \tag{46}$$

The force-balance boundary conditions [Eqs. (8) and (10), appropriate for bubbles] lead to

$$\frac{\partial v_r}{\partial \theta} + r\frac{\partial v_\theta}{\partial r} - v_\theta = 0 \; at \; r = R, \tag{47}$$

$$-p + 2\eta \frac{\partial v_r}{\partial r} = \frac{2\gamma}{R} + \frac{\gamma}{R^2}(l-1)(l+2) f(t) P_l(\cos\theta) \text{ at } r = R. \tag{48}$$

Substituting Eqs. (44) – (46) into Eqs. (47) and (48) and expressing the results in Laplace space, we find

$$(l-1)(l+1)\hat{\bar{C}}(s) + l(l+2)\hat{\bar{D}}(s) = 0, \tag{49}$$

$$\frac{l^2+3l-1}{l+1}\hat{\bar{C}}(s)+(l+2)\hat{\bar{D}}(s)=\frac{\gamma}{2\eta R^2}(l-1)(l+2)\hat{f}_l(s), \tag{50}$$

where $\bar{C}(t)=C(t)R^{-l-1}$ and $\bar{D}(t)=D(t)R^{-l-3}$. Using Eq. (44) in Eq. (41b), the kinematic boundary condition in Laplace space, we obtain

$$s\hat{f}_l(s)=f_l(0)-[\hat{\bar{C}}(s)+\hat{\bar{D}}(s)]R. \tag{51}$$

Solving the last three equations, we find

$$\hat{\bar{C}}(s)=\frac{\frac{\gamma}{R^2}l(l-1)(l+1)(l+2)f_l(0)}{2\eta s(2l^2+1)+\frac{\gamma}{R}(l-1)(l+1)(2l+1)}, \tag{52a}$$

$$\hat{\bar{D}}(s)=-\frac{\frac{\gamma}{R^2}(l-1)^2(l+1)^2f_l(0)}{2\eta s(2l^2+1)+\frac{\gamma}{R}(l-1)(l+1)(2l+1)}, \tag{52b}$$

$$\hat{f}_l(s)=\frac{2\eta(2l^2+1)f_l(0)}{2\eta s(2l^2+1)+\frac{\gamma}{R}(l-1)(l+1)(2l+1)}=\frac{f_l(0)}{s+\lambda_l^{\mathrm{B}}}. \tag{52c}$$

This $\hat{f}_l(s)$ corresponds an exponential function of time, with the recovery rate λ_l^{B} given by Eq. (17).

We also solve the full problem where both interior and exterior fluid dynamcis are treated. The derivation is presented in Appendix A, and the final reuslt for the shape deformation is

$$\hat{f}_l(s)=\frac{f_l(0)}{s+\lambda_l}, \tag{53}$$

where the recovery rate λ_l is given by Eq. (20a).

III. INTERFACE SHAPE RCOVERY: VISCOELASTIC FLUIDS

A. Constitutive relation for viscoelastic fluids

In Newtonian fluids, shear relaxation occurs instantaneously, and hence the stress responds only to the strain rate at the same moment [see Eq. (3b)]. For later reference, we present this constitutive relation in Laplace space:

$$\hat{\tilde{\tau}}_{\mathrm{d}}(s) = \eta \hat{\tilde{\varepsilon}}(s). \tag{54}$$

In biomolecular condensates and other complex materials, shear relaxation occurs at a finite rate [12,20,21,36,37], and consequently the stress depends on the entire history of the strain rate. Limiting to small strain rates so that the relation between $\tilde{\tau}_{\mathrm{d}}$ and $\tilde{\varepsilon}$ remains linear, Eq. (3b) is generalized to [21]

$$\tilde{\tau}_{\mathrm{d}}(t) = \int_{-\infty}^{t} dt' G(t-t')\, \tilde{\varepsilon}(t'). \tag{55a}$$

$$= \tilde{\tau}_{\mathrm{d}}(0) + \int_{0}^{t} dt' G(t-t')\, \tilde{\varepsilon}(t'). \tag{55b}$$

The function $G(t)$ introduced above is the shear relaxation modulus. For our problem at hand, the strain rate starts at $t = 0$ [i.e., $\tilde{\varepsilon}(t') = 0$ for $t' < 0$], and hence

$$\tilde{\tau}_{\mathrm{d}}(0) = 0 \tag{55c}$$

and Eq. (55b) becomes

$$\tilde{\tau}_{\mathrm{d}}(t) = \int_{0}^{t} dt' G(t-t')\, \tilde{\varepsilon}(t'). \tag{55d}$$

Note that we must also have $G(t') = 0$ for $t' < 0$ since otherwise Eq. (55a) would mean that future strain rates [$\tilde{\varepsilon}(t')$ at $t' > t$] would affect the present stress $\tilde{\tau}_{\mathrm{d}}(t)$. Taking the Laplace transform of Eq. (55d), we obtain a simple constitutive relation between $\hat{\tilde{\tau}}_{\mathrm{d}}$ and $\hat{\tilde{\varepsilon}}$:

$$\hat{\tilde{\tau}}_{\mathrm{d}}(s) = \hat{G}(s)\hat{\tilde{\varepsilon}}(s). \tag{55e}$$

In comparison to Eq. (54) for Newtonian fluids, we see that the only difference is that η is now replaced with $\hat{G}(s)$. Therefore, in Laplace space, the Navier-Stokes equations can be generalized to viscoelastic fluids by simply replacing η with $\hat{G}(s)$! Correspondingly, the solution for Newtonian fluids can be transformed to the solution for viscoelastic fluids by the same replacement. We will present this solution in the next subsections.

The Fourier transform of $G(t)$ defines the complex shear modulus, $G^*(\omega)$, where ω is the angular frequency. We have the following relation:

$$G^*(\omega) = i\omega\hat{G}(i\omega). \tag{56}$$

where i is the unit imaginary number.

We now introduce various models of linear viscoelasticity. The constitutive relation, Eq. (3b), for Newtonian fluids corresponds to a delta function for the shear relaxation modulus:

$$G(t) = \eta\delta(t - 0^+), \tag{57}$$

where 0^+ indicates a peak position that is beyond $t = 0$ by an arbitrarily small positive amount. The Laplace transform of this $G(t)$ is η, thus validating that Eq. (55e) properly reduces to Eq. (54) when the fluids are Newtonian. In the so-called Maxwell model, shear relaxation is an exponential function of time, with a time constant τ^{sr},

$$G(t) = \frac{\eta}{\tau^{\mathrm{sr}}} e^{-t/\tau^{\mathrm{sr}}} \text{ for } t > 0. \tag{58}$$

The Laplace transform is

$$\hat{G}(s) = \frac{\eta}{1 + \tau^{\mathrm{sr}} s}. \tag{59}$$

In the limit $\tau^{\mathrm{sr}} \to 0$, the Maxwell model reduces to a Newtonian fluid, consistent with the latter's instantaneous shear relaxation. A linear combination of a Newtonian fluid and the Maxwell model,

$$\hat{G}(s) = \eta_0 + \frac{\eta_1}{1 + \tau_1^{\mathrm{sr}} s}, \tag{60}$$

is the Jeffreys model, which also been seen as the linearized version of the Oldroyd B model. When the Newtonian component of Eq. (60) is also generalized to be Maxwellian, i.e.,

$$\hat{G}(s) = \frac{\eta_0}{1 + \tau_0^{\mathrm{sr}} s} + \frac{\eta_1}{1 + \tau_1^{\mathrm{sr}} s}, \tag{61}$$

we obtain the Burgers model. In Eq. (61), we assume $\tau_0^{\mathrm{sr}} < \tau_1^{\mathrm{sr}}$. The value of $\hat{G}(s)$ at $s = 0$ will be particularly useful. We call it the zero-frequency viscosity and denote it as

$$\eta_{\mathrm{z}} \equiv \hat{G}(0). \tag{62a}$$

For the Jeffreys and Burgers models, the zero-frequency viscosity is

$$\eta_{\mathrm{z}} = \eta_0 + \eta_1. \tag{62b}$$

We can represent an arbitrary shear relaxation modulus by adding more and more Maxwellian components. However, these more complicated models rarely are useful.

B. Shape recovery dynamics: viscoelastic droplets in an ideal fluid

By substituting the shear relaxation modulus $\hat{G}(s)$ for the viscosity η in Eq. (42c), we obtain the shape deformation amplitude, $\hat{f}_l(s)$, for viscoelastic droplets,

$$\hat{f}_l(s) = \frac{f_l(0)}{s + \lambda_l^{\mathrm{D}}/\hat{g}(s)}, \tag{63}$$

where λ_l^{D} is given by Eq. (15) but with η now replaced by $\eta_{\mathrm{z}} \equiv \hat{G}(0)$ [eq (62a)], i.e.,

$$\lambda_l^{\mathrm{D}} = \frac{l(l+2)(2l+1)}{2(2l^2+4l+3)} \frac{\gamma}{\eta_{\mathrm{z}} R}, \tag{64}$$

and

$$\hat{g}(s) = \frac{\hat{G}(s)}{\eta_{\mathrm{z}}}. \tag{65}$$

Note that the area under the $f_l(t)$ vs. t curve, given by $\hat{f}_l(0)$, is

$$\hat{f}_l(0) = \frac{f_l(0)}{\lambda_l^{\mathrm{D}}}. \tag{66}$$

With this result, we can interpret λ_l^{D} as the mean recovery rate, in that the exponential function $f_l(0)e^{-\lambda_l^{\mathrm{D}} t}$ has the same area as $f_l(t)$. Equation (66) is derived by realizing that $\hat{g}(0) = 1$, which is true by definition. Because Eq. (66) holds regardless of the form of $\hat{g}(s)$, the area of the $f_l(t)$ curve must be conserved when the parameters in $\hat{g}(s)$ or even the functional form of $\hat{g}(s)$ is varied, including the Newtonian fluid, which is specified by $\hat{g}(s) = 1$.

C. Shape recovery dynamics: ideal-fluid bubbles in a viscoelastic medium

Similarly, by substituting the shear relaxation modulus $\hat{G}(s)$ for the viscosity η in Eq. (52c), we obtain the shape deformation amplitude, $\hat{f}_l(s)$, for ideal-fluid bubbles in a viscoelastic medium,

$$\hat{f}_l(s) = \frac{f_l(0)}{s + \lambda_l^{\mathrm{B}}/\hat{g}(s)}, \tag{67}$$

where λ_l^{B} is given by Eq. (17) but with η now replaced by η_{z},

$$\lambda_l^{\mathrm{B}} = \frac{(l-1)(l+1)(2l+1)}{2(2l^2+1)} \frac{\gamma}{\eta_{\mathrm{z}} R}, \tag{68}$$

and represents the mean recovery rate that corresponds to the area under the $f_l(t)$ vs. t curve.

D. Shape recovery dynamics: viscoelastic fluids

For the shape recovery of a deformed viscoelastic droplet in a viscous fluid, by substituting $\hat{G}_{\mathrm{II}}(s)$ for the interior viscosity η_{II} in λ_l that is given by Eq. (20a) and appears in Eq. (53), we obtain

$$\hat{f}_l(s) = \frac{f_l(0)}{s + \lambda_l^{\mathrm{I}}/h_l(s)}, \tag{69a}$$

where

$$\lambda_l^{\mathrm{I}} = \frac{e_l \gamma}{\eta_{\mathrm{I}} R}, \tag{69b}$$

$$h_l(s) = \frac{\left[a_l \alpha_{\mathrm{II/I}} \hat{g}_{\mathrm{II}}(s) + b_l\right]\left[c_l \alpha_{\mathrm{II/I}} \hat{g}_{\mathrm{II}}(s) + d_l\right]}{\alpha_{\mathrm{II/I}} \hat{g}_{\mathrm{II}}(s) + 1}, \tag{69c}$$

with a_l, b_l, c_l, d_l, and e_l given by Eqs. (20b-f). Furthermore, $\alpha_{\mathrm{II/I}}$ is the viscosity ratio given by Eq. (20g) but η_{II} now represents the zero-frequency viscosity of the viscoelastic droplet, and

$$\hat{g}_{\mathrm{II}}(s) = \frac{\hat{G}_{\mathrm{II}}(s)}{\eta_{\mathrm{II}}}. \tag{69d}$$

At $s = 0$, we find

$$\hat{f}_l(0) = \frac{f_l(0)}{\lambda_l^{\mathrm{I}}/h_l(0)} = \frac{f_l(0)}{\lambda_l}, \tag{69e}$$

where λ_l is given by Eq. (20a). Equation (69e) means that the area under the $f_l(t)$ curve is conserved for any $\hat{g}_{II}(s)$, including the one, $\hat{g}_{II}(s) = 1$, for Newtonian fluids.

The foregoing results can also apply to the reverse case, i.e., a viscous droplet in a viscoelastic medium, after the following changes: replacing λ_l^{I} with λ_l^{II} and $\hat{g}_{\mathrm{II}}(s)$ with $\hat{g}_{\mathrm{I}}(s)$, and swapping a_l with b_l and c_l with d_l in Eq. (69c). Finally the shape recovery dynamics of the most general case, i.e., a viscoelastic droplet in a viscoelastic medium, can be obtained by further modifying λ_l in Eq. (53). This time, the modification entails substituting both $\hat{G}_{\mathrm{II}}(s)$ for the interior viscosity η_{II} and $\hat{G}_{\mathrm{I}}(s)$ for the exterior viscosity η_{I} in the expression of λ_l given by Eq. (20a).

IV. ILLUSTRATIVE RESULTS AND DISCUSSION

The analytical solution in the preceding two sections predicts rich dynamic behaviors of deformed droplets during their shape recovery. Here we present illustrative results, to motivate experimental studies into the effects of viscoelasticity on shape dynamics of biomolecular condensates, and demonstrate the potential importance of the present analytical solution in fitting experimental data and in validating numerical solutions.

A. COMPARISON BETWEEN DROPLET AND FUSION AND SHAPE RECOVERY

It is interesting to compare the dynamics of the two kinds of shape changes: fusion of two droplets and recovery of a deformed droplet. The half-length, $L_{\mathrm{fus}}(t)$, of two fusing viscous droplets, initially with equal radius R, in an ideal-fluid medium is approximately given by [26]

$$L_{\mathrm{fus}}(t) - L_{\mathrm{fus}}(\infty) = [L_{\mathrm{fus}}(0) - L_{\mathrm{fus}}(\infty)]e^{-(t/\tau_{\mathrm{fus}})^{\beta}}, \tag{70}$$

where $\beta = 1.5$ and

$$\tau_{\mathrm{fus}} = 1.97\frac{\eta R}{\gamma} \equiv 1.97\tau^{\mathrm{vc}}. \tag{71}$$

The last identity defines the viscocapillary time τ^{vc}. For the shape recovery of a deformed droplet, the half-length is given by [Eq. (14)]

$$L_{\mathrm{rec}}(t) - L_{\mathrm{rec}}(\infty) = f_l(t) = [L_{\mathrm{rec}}(0) - L_{\mathrm{rec}}(\infty)]e^{-\lambda_l^{\mathrm{D}} t}. \tag{72}$$

The relaxation rate for $l = 2$ and 4 are [Eq. (15)]

$$\lambda_2^{\mathrm{D}} = \frac{20}{19\tau^{\mathrm{vc}}}, \tag{73a}$$

$$\lambda_4^{D} = \frac{36}{17\tau^{\mathrm{vc}}}. \tag{73b}$$

As Fig. 2 shows, the fusion dynamics is a stretched exponential function of time, occurring more slowly than the shape recovery dynamics of a droplet with a deformation represented by the lowest-order Legendre polynomial ("P2"). As the order of the Legendre polynomial increases, shape recovery becomes even faster. Hubstenberger et al. [1] have indeed observed that, after deformation, shape recovery of grP-bodies formed in the cytoplasm of *Caenorhabditis elegans* oocytes occurred on a much shorter timescale than the fusion of these ribonucleoprotein condensates. However, Fig. 2 shows that the results predicted for viscous droplets are unlikely to reach the two orders of magnitude difference in timescales reported by Hubstenberger et al. These authors suggested that viscoelasticity may play a role. Next we presents results for viscoelastic droplets.

B. SHAPE RECOVERY OF VISCOELASTIC DROPELTS

We now examine the time dependence of $f_l(t)$ for viscoelastic droplets in an ideal fluid. For the Maxwell model of linear viscoelasticity, substituting Eq (59) into Eq. (63) yields

$$\hat{f}_l(s) = \frac{f_l(0)}{s + \lambda_l^{\mathrm{D}}(1 + \tau^{\mathrm{sr}} s)} = \frac{f_l(0)/(1 + \tau^{\mathrm{sr}}\lambda_l^{\mathrm{D}})}{s + \lambda_l^{\mathrm{D}}/(1 + \tau^{\mathrm{sr}}\lambda_l^{\mathrm{D}})}. \tag{74}$$

The inverse Laplace transform is

$$f_l(t) = \frac{f_l(0)}{1 + \tau^{\mathrm{sr}}\lambda_l^{\mathrm{D}}} e^{-\lambda_l^{\mathrm{D}} t/(1+\tau^{\mathrm{sr}}\lambda_l^{\mathrm{D}})} \text{ for } t > 0^+, \tag{75}$$

which is an exponential function of time. The recovery rate, $\lambda_l^{\mathrm{D}}/(1 + \tau^{\mathrm{sr}}\lambda_l^{\mathrm{D}})$, is less than the counterpart for a Newtonian fluid (when $\tau^{\mathrm{sr}} = 0$) by a factor of $1 + \tau^{\mathrm{sr}}\lambda_l^{\mathrm{D}}$. The apparent zero-time deformation, $f_l(0)/(1 + \tau^{\mathrm{sr}}\lambda_l^{\mathrm{D}})$, is also less than the nominal value, $f_l(0)$, by the same factor, as required by the conservation of area under the curve [see Eq. (66)]. So evidently there is a missing amplitude of $f_l(0) - f_l(0)/(1 + \tau^{\mathrm{sr}}\lambda_l^{\mathrm{D}}) = [\tau^{\mathrm{sr}}\lambda_l^{\mathrm{D}}/(1 + \tau^{\mathrm{sr}}\lambda_l^{\mathrm{D}})]f_l(0)$; we elaborate its origin in Appendix B. This can be traced to $\hat{G}(\infty) = 0$ for the Maxwell model. The 0 value of $\hat{G}(\infty)$ violates an assumption used for deriving Eq. (74), which is that $\hat{G}(s)$ is much greater than the exterior viscosity. The full solution without this assumption does not suffer from this artifact.

Next we consider the Jeffreys model. Substituting Eq. (60) into Eq. (63) gives

$$\hat{f}_l(s) = \frac{\left(\eta_0 + \frac{\eta_1}{1 + \tau_1^{\mathrm{sr}} s}\right) f_l(0)}{s\left(\eta_0 + \frac{\eta_1}{1 + \tau_1^{\mathrm{sr}} s}\right) + \eta_{\mathrm{z}}\lambda_l^{\mathrm{D}}}. \tag{76}$$

The inverse Laplace transform of Eq. (76) is a sum of two exponentials as opposed to a single exponential for a Newtonian or Maxwellian fluid. The two exponentials are

$$f_l(t) = f_l(0)\left(A_{l+} e^{-\lambda_{l+}^{\mathrm{D}} t} + A_{l-} e^{-\lambda_{l-}^{\mathrm{D}} t}\right) \tag{77a}$$

where

$$\lambda_{l\pm}^{\mathrm{D}} = \frac{1}{2(\eta_0/\eta_{\mathrm{z}})\tau_1^{\mathrm{sr}}}\left[\tau_1^{\mathrm{sr}}\lambda_l^{\mathrm{D}} + 1 \pm \sqrt{(\tau_1^{\mathrm{sr}}\lambda_l^{\mathrm{D}} + 1)^2 - 4(\eta_0/\eta_{\mathrm{z}})\tau_1^{\mathrm{sr}}\lambda_l^{\mathrm{D}}}\right] \quad (77b)$$

$$A_{l\pm} = \frac{1}{2}\left[1 \pm \frac{\tau_1^{\mathrm{sr}}\lambda_l^{\mathrm{D}} - 1}{\sqrt{(\tau_1^{\mathrm{sr}}\lambda_l^{\mathrm{D}} + 1)^2 - 4(\eta_0/\eta_{\mathrm{z}})\tau_1^{\mathrm{sr}}\lambda_l^{\mathrm{D}}}}\right] \quad (77c)$$

In the limit $\eta_1 \to 0$, the two recovery rates of Eqs. (77b) reduce to λ_l^{D} and $1/\tau_1^{\mathrm{sr}}$, and the corresponding amplitudes given by Eq. (77c) reduce to 1 and 0, respectively. Thus Eq. (77a) properly reduces to the single exponential of Eq. (72) for a Newtonian fluid. In the limit $\eta_0 \to 0$, the two recovery rates become infinite and $\lambda_l^{\mathrm{D}}/(1 + \tau_1^{\mathrm{sr}}\lambda_l^{\mathrm{D}})$, and the corresponding amplitudes are $\tau_1^{\mathrm{sr}}\lambda_l^{\mathrm{D}}/(1 + \tau_1^{\mathrm{sr}}\lambda_l^{\mathrm{D}})$ and $1/(1 + \tau_1^{\mathrm{sr}}\lambda_l^{\mathrm{D}})$. This result for the $\eta_0 \to 0$ limit thus reveals that the missing amplitude of the Maxwell model is due to an instantaneous decay at $t = 0^+$, consistent with the analysis in Appendix B.

The scaled recovery rates $\lambda_{l\pm}^{\mathrm{D}}/\lambda_l^{\mathrm{D}}$ and the amplitudes $A_{l\pm}$ depend only on two dimensionless parameters: η_0/η_{z} and $\tau_1^{\mathrm{sr}}\lambda_l^{\mathrm{D}}$. It can be easily shown that $\lambda_{l+}^{\mathrm{D}}/\lambda_l^{\mathrm{D}} > 1$ whereas $\lambda_{l-}^{\mathrm{D}}/\lambda_l^{\mathrm{D}} < 1$ for all parameter values. For a given η_0/η_{z}, $\tau_1^{\mathrm{sr}}\lambda_l^{\mathrm{D}} = 1$ is a special point, where A_{l+}/A_{l-} is 1 and $\lambda_{l+}^{\mathrm{D}}/\lambda_{l-}^{\mathrm{D}}$ reaches its minimum. The equality in amplitude between the two exponentials makes the $f_l(t)$ curve at $\tau_1^{\mathrm{sr}}\lambda_l^{\mathrm{D}} = 1$ appear most strongly non-exponential. At this special $\tau_1^{\mathrm{sr}}\lambda_l^{\mathrm{D}}$, $\lambda_{l+}^{\mathrm{D}}$ and $\lambda_{l-}^{\mathrm{D}}$ get closer and closer to each other as η_0/η_{z} approaches 1, i.e., when the Newtonian component of the complex shear modulus becomes dominant. In Fig. 3 we compare the shape recovery curves at η_0/η_1 = 5:1, 1:1, and 1:5. Whereas the curve at η_0/η_1 = 5:1 is close to the counterpart of Newtonian droplets, the curve at η_0/η_1 = 1:5 is clearly non-exponential, with a fast decay followed by a slow decay. The curve at η_0/η_1 = 1:1 is intermediate between those two.

Recently we have found that modulating intermolecular interactions, e.g., by adding salt, can tune the η_0/η_1 ratio [21]. For PGL-3 protein droplets, the Maxwellian component dominates (i.e., $\eta_0/\eta_1 < 1$) at low salt while the Newtonian component dominates (i.e., $\eta_0/\eta_1 > 1$) at high salt. Qualitatively, we expect that shape recovery curves of PGL-3 droplets to become less non-exponential at increasing salt concentration. Experimental studies of salt effects on the shape recovery dynamics of biomolecular condensates will be of particular interest. Salts also have complex effects on the shear relaxation moduli of polymer blends [43].

Finally let us consider the Burgers model. Substituting Eq. (61) into Eq. (63) yields

$$\hat{f}_l(s) = \frac{\left(\frac{\eta_0}{1+\tau_0^{\mathrm{sr}}s} + \frac{\eta_1}{1+\tau_1^{\mathrm{sr}}s}\right) f(0)}{s\left(\frac{\eta_0}{1+\tau_0^{\mathrm{sr}}s} + \frac{\eta_1}{1+\tau_1^{\mathrm{sr}}s}\right) + \eta_{\mathrm{z}}\lambda_l^{\mathrm{D}}} \tag{78}$$

The inverse Laplace transform again gives $f_l(t)$ as a bi-exponential like Eq. (77a). The Burgers model has $\hat{G}(\infty) = 0$, and correspondingly there is also a missing amplitude, by a factor of $\eta_{\mathrm{z}}\tau_0^{\mathrm{sr}}\tau_1^{\mathrm{sr}}\lambda_l^{\mathrm{D}}/(\eta_0\tau_1^{\mathrm{sr}} + \eta_1\tau_0^{\mathrm{sr}} + \eta_{\mathrm{z}}\tau_0^{\mathrm{sr}}\tau_1^{\mathrm{sr}}\lambda_l^{\mathrm{D}})$. The two recovery rates and the corresponding amplitudes can be found in Appendix C.

The foregoing results for viscoelastic droplets in an ideal fluid also apply to the shape recovery dynamics of ideal-fluid bubbles in a viscoelastic medium, after replacing λ_l^{D} with λ_l^{B}. The expressions for these two relaxation rates are given in Eqs. (64) and (68), respectively. From here on, we will focus on the Jeffreys model of linear viscosity.

C. EFFECT OF SHEAR RELAXATION RATE

Let us look closely at the effect of τ_1^{sr}, the shear relaxation rate in the Jeffreys model, on the shape recovery dynamics of viscoelastic droplets in an ideal fluid. First consider the

two limiting cases. For extremely fast shear relaxation, i.e., $\tau_1^{\mathrm{sr}}\lambda_l^{\mathrm{D}} \ll 1$, expanding Eqs. (77b) and (77c) in powers of $\tau_1^{\mathrm{sr}}\lambda_l^{\mathrm{D}}$ and keeping terms up to the first power, we find

$$\lambda_{l+}^{\mathrm{D}} \approx \frac{1}{(\eta_0/\eta_{\mathrm{z}})\tau_1^{\mathrm{sr}}} + \frac{\eta_1}{\eta_0}\lambda_l^{\mathrm{D}};\ \lambda_{l-}^{\mathrm{D}} \approx \lambda_l^{\mathrm{D}} \tag{79}$$

$$A_{l+} \approx \frac{\eta_1}{\eta_{\mathrm{e}}}\tau_1^{\mathrm{sr}}\lambda_l^{\mathrm{D}};\ A_{l-} \approx 1 - \frac{\eta_1}{\eta_{\mathrm{e}}}\tau_1^{\mathrm{sr}}\lambda_l^{\mathrm{D}} \tag{80}$$

The first exponential, $A_{l+}e^{-\lambda_{l+}^{\mathrm{D}}t}$, has a small amplitude and decays rapidly to 0, and hence is less important. The remaining exponential, $A_{l-}e^{-\lambda_{l-}^{\mathrm{D}}t}$, has an amplitude close to 1 and a recovery rate of λ_l^{D}. Hence under extremely fast shear relaxation the droplet behaves as if it is a Newtonian fluid, as expected by setting $\tau_1^{\mathrm{sr}} = 0$ in Eq. (60).

In the opposite limit where shear relaxation is extremely slow, i.e., $\tau_1^{\mathrm{sr}}\lambda_l^{\mathrm{D}} \gg 1$, we expand Eqs. (77b) and (77c) in powers of $1/\tau_1^{\mathrm{sr}}\lambda_l^{\mathrm{D}}$ and keep terms up to the first power, finding

$$\lambda_{l+}^{\mathrm{D}} \approx \frac{\eta_{\mathrm{z}}}{\eta_0}\lambda_l^{\mathrm{D}} + \frac{\eta_1}{\eta_0}\frac{1}{\tau_1^{\mathrm{sr}}};\ \lambda_{l-}^{\mathrm{D}} \approx \frac{1}{\tau_1^{\mathrm{sr}}} \tag{81}$$

$$D_{+;l} = 1 - \frac{\eta_1}{\eta_{\mathrm{z}}}(\tau_1^{\mathrm{sr}}\lambda_l^{\mathrm{D}})^{-1};\ D_{-;l} = \frac{\eta_1}{\eta_{\mathrm{z}}}(\tau_1^{\mathrm{sr}}\lambda_l^{\mathrm{D}})^{-1} \tag{82}$$

In this case, the first exponential has an amplitude that is close to 1 and a recovery rate of the order of λ_l^{D}, while the second exponential has a very small amplitude but a very slow recovery rate, $1/\tau_1^{\mathrm{sr}}$. The ratio of the areas under the two exponentials is approximately η_0/η_1 and hence both areas can be significant, but the second, slow exponential may be difficult to detect experimentally due to the small amplitude, therefore giving the false impression of fast shape recovery. This finding could provide an explanation for the shorter than expected timescale of grP-body shape recovery observed by Hubstenberger et al. [1].

In Fig. 4, we display shape recovery curves for η_0/η_1 at 1:5 and $\tau_1^{\mathrm{sr}}\lambda_l^{\mathrm{D}}$ at 0.1, 1, 10, and 50. In all the cases, $f_l(t)$ exhibits a fast initial decay followed by a slow second decay. With increasing τ_1^{sr}, the amplitude of the initial decay becomes larger and that of the second decay becomes smaller, while the time constants of both decays become longer. Starting at $\tau_1^{\mathrm{sr}}\lambda_l^{\mathrm{D}} = 1$, the second time constant becomes dominated by shear relaxation and less and less dependent on interfacial tension. This finding challenges the currently prevailing viscocapillarity-centric view derived from purely viscous fluids.

As noted in the preceding subsection, the results illustrated by Fig. 4 are also applicable to the shape recovery of bubbles in a viscoelastic medium upon replacing λ_l^{D} with λ_l^{B}. Ali and Prabhu [37] recently presented such data where the viscoelastic medium is coacervates formed by potassium poly(styrenesulfonate) and poly(diallyl dimethylammonium bromide). They observed an initial decay followed by a slow second decay, qualitatively in agreement with our prediction. The shear relaxation in their system has $\tau_1^{\mathrm{sr}} < 1$ s and becomes faster with increasing salt (similar to results found for PGL-3 droplets [21]). In comparison, the time constants of their second decay, corresponding to our $1/\lambda_{l-}^{\mathrm{B}}$, are mostly > 1 s. Ali and Prabhu analyzed their data essentially by assuming $\lambda_{l-}^{\mathrm{B}} = \lambda_l^{\mathrm{B}}$, i.e., completely neglecting shear relaxation. However, even fast shear relaxation can affect $\lambda_{l-}^{\mathrm{B}}$, and hence its neglect can lead to underestimation of the interfacial tension. For example, at $\tau_1^{\mathrm{sr}}\lambda_l^{\mathrm{B}} = 0.1$, we predict $\lambda_{l-}^{\mathrm{B}} = 0.92\lambda_l^{\mathrm{B}}$. Ali and Prabhu also reported the time, t_{e}, for the initial decay to complete. t_{e} should scale with $1/\lambda_{l+}^{\mathrm{B}}$, i.e., the time constant of the initial decay, which we predict to be significantly affected by the shear relaxation rate [see $\lambda_{l+}^{\mathrm{D}}$ given by Eq. (79)]. Indeed, Ali and Prabhu reported an approximately 10-fold decrease in t_{e} when the salt concentration increased from 1.55 to 1.85 M. Over the same range of salt concentration, the time constants

of their decay changed by < 2-fold whereas the shear relaxation rates changed substantially, suggesting their major role in determining t_{e}.

D. FINITE VISCOSITY RATIO: NEWTONIAN FLUIDS

So far we have only considered cases where either the interior or the exterior fluid dynamics is important. Now we want to present cases where the viscosity ratio between the two phases is finite so that both interior and the exterior fluid dynamics must be treated at the same time. As a prelude to cases where a viscoelastic phase interfaces with a viscous phase, here we first consider the case where both of the phases are viscous. The shape recovery dynamics is an exponential function [see Eq. (53)], with the recovery rate λ_l given by Eq. (20a). For $l = 2$, the recovery rate is

$$\lambda_2 = \frac{40(\eta_{\mathrm{II}}/\eta_{\mathrm{I}} + 1)}{(19\eta_{\mathrm{II}}/\eta_{\mathrm{I}} + 16)(2\eta_{\mathrm{II}}/\eta_{\mathrm{I}} + 3)} \frac{1}{\tau_{\mathrm{I}}^{\mathrm{vc}}}, \tag{83a}$$

where

$$\tau_{\mathrm{I}}^{\mathrm{vc}} = \frac{\eta_{\mathrm{I}} R}{\gamma}. \tag{83b}$$

Equation (83a) is identical to the recovery rate widely quoted for droplets approximated as ellipsoids [29,30,32,34,37].

Although shapes specified by the second-order Legendre polynomial ("P2") have been assumed to be equivalent to ellipsoids [e.g., 44], there are actually noticeable differences between them. As detailed in Appendix D, P2 combined with a small amplitude fourth-order Legendre polynomial (P4) does an excellent job in reproducing ellipsoidal shapes. A deformation with an ellipsoidal shape thus requires a linear combination of $f_2(t)$ and $f_4(t)$ (see Fig. 2), leadging to a bi-exponential decay even when both phases are Newtonian fluids.

For the rest of the paper, we will limit to $l = 2$, focusing attention instead on non-exponentiality arising from viscoelasticity.

In Fig. 5(a) we present the shape recovery curves for Newtonian droplets in a Newtonian fluid with $\eta_{\mathrm{II}}/\eta_{\mathrm{I}}$ at 10, 1.5, and 0.5. This will serve as references for assessing the effect of droplet viscosity in the next subsection. One can tune $\eta_{\mathrm{II}}/\eta_{\mathrm{I}}$ by changing temperature or salt concentration. In cases where the dense phase is inside droplets, $\eta_{\mathrm{II}}/\eta_{\mathrm{I}}$ away from critical point is much higher than 1 and approaches 1 as the critical point is reaches. For complex biomolecular condensates, one also tune $\eta_{\mathrm{II}}/\eta_{\mathrm{I}}$ by varying their macromolecular composition [16,18,26].

E. FINITE VISCOSITY RATIO: VISCOELASTIC FLUIDS

To determine the shape recovery dynamics of viscoelastic droplets in a Newtonian fluid, we obtain $f_l(t)$ of Eq. (69a) by numerical Laplace inversion [45]. The results are displayed as dotted curves in Fig. 5(a) for Jeffreys droplets with $\eta_{\mathrm{II0}}/\eta_{\mathrm{II1}}$ at 1:5, $\tau_{\mathrm{II1}}^{\mathrm{sr}}\gamma/\eta_{\mathrm{I}}R$ at 10, and $\eta_{\mathrm{II}}/\eta_{\mathrm{I}}$ at 10, 1.5, and 0.5. Similar to the results presented in Figs. 3 and 4 for $\eta_{\mathrm{II}}/\eta_{\mathrm{I}} = \infty$, for each finite $\eta_{\mathrm{II}}/\eta_{\mathrm{I}}$ value, the initial decay of $f_l(t)$ for the Jeffreys droplet ("J/N") is faster than that of the corresponding Newtonian droplet ("N/N"). The J/N curve then slows down and crosses the N/N curve.

It is interesting to compare the shape recovery curves between Jeffreys droplets in a Newtonian fluid (i.e., "J/N") and Newtonian droplets in a viscoelastic medium ("N/J"). The N/J results are shown as dashed curves in Fig. 5(a). When $\eta_{\mathrm{II}}/\eta_{\mathrm{I}} > 1$, relative to the J/N curves, the corresponding N/J curves move closer to the N/N curves. Conversely, when $\eta_{\mathrm{II}}/\eta_{\mathrm{I}} < 1$, it is the J/N curves that are closer to the N/N curves. At $\eta_{\mathrm{II}}/\eta_{\mathrm{I}} = 1.5$ and 0.5, with

$\tau_1^{\mathrm{sr}}\gamma/\eta_{\mathrm{I}}R = 10$, the shear relaxation of the viscoelastic fluids occurs on a timescale that is apprximately 10 times longer than both the interior and exteruor viscocapillary times. Correspondingly, the shape recovery curves at $\eta_{\mathrm{II}}/\eta_{\mathrm{I}} = 1.5$ and 0.5 all have a slow decay with a time constant close to τ_1^{sr}. So once again we observe the scenario where the slowest decay is dictated by shear relaxation and independent of interfacial tension.

In Fig. 5(b), we compare our analytical solution with the experimental data of Verhulst et al. [36] for N/N, J/N, and N/J systems, all with $\eta_{\mathrm{II}}/\eta_{\mathrm{I}} = 1.5$. Our prediction for the N/N system is accurate. Compared with our result for the J/N system, the experimental curve did not deviate as much from that of the N/N system. On the other hand, the experimental curve for the N/J system showed a much more pronounced slow decay than our prediction. We speculate that the discrepancies for the two viscoelastic systems may be attributed to the neglect of inertial effects in our solution. Inertial effects can be accounted for by modifying the full solution of Prosperetti [28] [Eqs. (18) to (19c)] with $\hat{G}_{\mathrm{II}}(s)$ substituting for η_{II} and/or $\hat{G}_{\mathrm{I}}(s)$ for η_{I} in Eq. (19c). We will pursue this lead in the future to investigate whether inertial effects are important for biomolecular condensates. What is important here is that the experimental data of Verhulst et al. for the N/J system provides evidence for a slow decay that is dictated by shear relaxation, as our analytical solution predicts.

We also compared our analytical solution with the work of Hooper at al. [31], who numerically solved the fluid-dynamics equations with the Oldroyd B constitutive relation. The analytical and numerical results agree well for Newtonian droplets in a Newtonian fluid. However, for viscoelastic droplets in a Newtonian fluid, Hooper et al.'s initial decay of the shape deformation is faster. Inertial effects have no role in this discrepancy since they are neglected in both studies. Although the analytical solution is limited to linear order

(specifically in the extent of shape deformation and in the linearization of the Oldroyd B model), it is possible that the numerical solution incurred errors. The Oldroyd B model is known to be difficult to implement numerically and to be prone to generate numerical instability [33]. Our analytical solution presents a unique benchmark to test the accuracy of numerical solutions.

V. CONCLUDING REMARKS

We have presented an exact analytical solution for the recovery dynamics of biomolecular droplets from small-amplitude deformation. Whereas viscocapillarity sets the timescale for the shape recovery dynamics of viscous droplets, with viscoelasticity, shape recovery becomes multi-exponential, involving decays in deformation that are both much faster and much slower than the viscocapillary timescale. In departure from the currently prevailing viscocapillarity-centric view, the slowest decay can be independent of interfacial tension but dictated by shear relaxation. A shear relaxation-dictated deformation decay has experimental support for from studies of polymer blends [36]. We anticipate qualitatively similar effects of shear relaxation on droplet fusion dynamics. Our theoretical results have also suggested a possible explanation for the disparity in timescale between droplet shape recovery and fusion reported by Hubstenberger et al. [1]. The explanation is that the fastest of the decays in deformation prevails in shape recovery whereas slower decays are also important in fusion. A full explanation will have to wait until viscoelasticity is also treated in calculating droplet fusion dynamics.

There is great interest in condensate aging, especially in its connection with neurodegeneration, but there is little physical understanding of this phenomenon. One

possible physical change of biomolecular condensates over time is the slowdown in shear relaxation [12]. Our analytical solution predicts that a slowdown in shear relaxation can lead to a very slow decay in shape dynamics, thereby giving the appearance of stalled or incomplete shape recovery and fusion. The work here thus reveals shear relaxation as a crucial link in understanding condensate aging.

Our analytical solution should prove useful for validating numerical solutions of fluid-dynamics equations for condensate shape changes. Such validation is important, as numerical solutions may be the only option for the theoretical treatment of nonlinear issues such as large-amplitude deformation and nonlinear constitutive relations (e.g., the Oldroyd B model). We do expect that our present solution is still qualitatively and even semi-quantitatively correct when nonlinearity is present, and as such will be good for fitting experimental data on shape recovery. Finally shape recovery and fusion may potentially be modeled by molecular simulations [44] and our analytical theory can motivate and guide data analysis in such studies.

ACKNOWLEDGMENTS

This work was supported by Grant GM118091 from the National Institutes of Health.

APPENDIX A: SOLUTION WHEN BOTH η_{I} AND η_{II} ARE FINITE

When both η_{I} and η_{II} are finite, we need to consider both the interior and exterior fluid dynamics. The boundary conditions on the interface between the droplet and bulk phases consist of the continuity of the velocity field,

$$\mathbf{v}_{\mathrm{II}} \cdot \mathbf{n} = \mathbf{v}_{\mathrm{I}} \cdot \mathbf{n}, \tag{A1a}$$

$$\mathbf{v}_{\mathrm{II}} \cdot \mathbf{t} = \mathbf{v}_{\mathrm{I}} \cdot \mathbf{t}, \tag{A1b}$$

the kinematic equation,

$$\frac{\partial \mathcal{S}}{\partial t} + \mathbf{v}_{\mathrm{II}} \cdot \nabla \mathcal{S} = 0, \tag{A2}$$

and the force-balance equations,

$$\mathbf{n} \cdot (\eta_{\mathrm{II}} \tilde{\varepsilon}_{\mathrm{II}} - \eta_{\mathrm{I}} \tilde{\varepsilon}_{\mathrm{I}}) \cdot \mathbf{t} = 0. \tag{A3a}$$

$$\mathbf{n} \cdot (\tilde{\boldsymbol{\tau}}_{\mathbf{II}} - \tilde{\boldsymbol{\tau}}_{\mathbf{I}}) \cdot \mathbf{n} = -\boldsymbol{\gamma} \boldsymbol{\nabla} \cdot \mathbf{n}, \tag{A3b}$$

The interior velocity and pressure fields are given by Eqs. (31) – (33); the exterior counterparts are given by Eqs. (44) – (46), except that the term $-\gamma/\eta R$ on the right-hand side of Eq. (46) should be removed, since the effect of this term is already accounted in Eq. (33) for the interior pressure. Equations (A1a) and (A1b) lead to

$$\hat{\hat{A}}(s) + \hat{\hat{B}}(s) = \hat{\hat{C}}(s) + \hat{\hat{D}}(s), \tag{A4a}$$

$$-(l+3)\hat{\hat{A}}(s) - (l+1)\hat{\hat{B}}(s) = (l-2)\hat{\hat{C}}(s) + l\hat{\hat{D}}(s). \tag{A4b}$$

Equation (A3a) leads to

$$\eta_{\mathrm{II}} \left[l(l+2)\hat{\hat{A}}(s) + (l-1)(l+1)\hat{\hat{B}}(s) \right]$$
$$= \eta_I \left[(l-1)(l+1)\hat{\hat{C}}(s) + l(l+2)\hat{\hat{D}}(s) \right]. \tag{A4c}$$

Equation (A3b) leads to

$$\eta_{\mathrm{II}} \left[\frac{l^2 - l - 3}{l} \hat{\hat{A}}(s) + (l-1)\hat{\hat{B}}(s) \right]$$
$$+\eta_I \left[\frac{l^2 + 3l - 1}{l+1} \hat{\hat{C}}(s) + (l+2)\hat{\hat{D}}(s) \right] = \frac{\gamma}{2R^2}(l-1)(l+2)\hat{f}(s). \tag{A4d}$$

Finally Eq. (A2) leads to Eq. (41b), which is

$$s\hat{f}_l(s) = f_l(0) - [\hat{\hat{A}}(s) + \hat{\hat{B}}(s)]R. \tag{A4e}$$

Solving Eqs. (A4a-e), we find the solution for $\hat{f}_l(s)$ given Eq. (53), with the recovery rate λ_l given by Eq. (20a).

APPENDIX B: MISSING AMPLITUDE OF MAXWELL DROPLETS

To find the origin of the missing amplitude of Maxwell droplets inside an ideal fluid, let us look at $\dot{f}_l(t)$, the rate of change in $f_l(t)$. Its Laplace transform is [using Eq. (41b) and Eqs. (42a, b) with η replaced by $\hat{G}(s)$]

$$s\hat{f}_l(s) - f_l(0) = -[\hat{\hat{A}}(s) + \hat{\hat{B}}(s)]R$$

$$= -\frac{\lambda_l^{\mathrm{D}} f_l(0)}{\frac{s}{1+\tau^{\mathrm{sr}}s} + \lambda_l^{\mathrm{D}}}$$

$$= -\frac{\tau^{\mathrm{sr}}\lambda_l^{\mathrm{D}} f_l(0)}{1+\tau^{\mathrm{sr}}\lambda_l^{\mathrm{D}}} - \frac{f_l(0)}{1+\tau^{\mathrm{sr}}\lambda_l^{\mathrm{D}}}\frac{\lambda_l^{\mathrm{D}}/(1+\tau^{\mathrm{sr}}\lambda_l^{\mathrm{D}})}{s+\lambda_l^{\mathrm{D}}/(1+\tau^{\mathrm{sr}}\lambda_l^{\mathrm{D}})}. \tag{B1}$$

The inverse Laplace transform is

$$\dot{f}_l(t) = -\frac{\tau^{\mathrm{sr}}\lambda_l^{\mathrm{D}} f_l(0)}{1+\tau^{\mathrm{sr}}\lambda_l^{\mathrm{D}}}\delta(t-0^+)$$

$$-\frac{f_l(0)}{1+\tau^{sr}\lambda_l^{D}}\frac{\lambda_l^{D}}{1+\tau^{sr}\lambda_l^{D}}e^{-\lambda_l^{D}t/(1+\tau^{sr}\lambda_l^{D})}. \tag{B2}$$

Upon integrating Eq. (B2) over time, the first term, a delta function, leads to an instantaneous drop in the amplitude at $t = 0^+$, which is exactly the missing amplitude; the second term yields the result in Eq. (75), which is applicable for $t > 0^+$.

In general, the behavior of $f_l(t)$ near $t = 0$ is dictated by $\hat{f}_l(s)$ at $s \to \infty$. If $\hat{G}(\infty)$ is a nonzero finite value, then the asymptote of $\hat{f}_l(s)$ given by Eq. (63) is $f_l(0)/s$, which upon inverse Laplace transform yields the correct value, $f_l(0)$, for $f_l(t)$ at $t = 0$. However, this analysis breaks down when if $\hat{G}(\infty) = 0$, as is the case for the Maxwell and Burgers models,

leading to the missing amplitude. Note that the 0 value of $\hat{G}(\infty)$ violates an assumption used for deriving Eq. (63), which is that $\hat{G}(s)$ is much greater than the exterior viscosity. The full solution, given by Eq. (69a), that accounts for the exterior viscosity does not suffer a missing amplitude. When $\hat{g}_{\mathrm{II}}(\infty) = 0$ as in the Maxwell and Burgers models, Eq. (69c) still yields a finite $h_l(\infty)$ and therefore Eq. (69a) gives the correct asymptote $f_l(0)/s$ for $\hat{f}_l(s)$.

APPENDIX C: SHAPE RECOVERY DYNAMICS OF BURGERS DROPLETS

For viscoelastic droplets modeled by the Burgers model, the inverse Laplace transform of Eq. (78) yields the bi-exponential form of Eq. (77a) for the shape recovery dynamics. The two recovery rates and the corresponding amplitudes are

$$\lambda_{l\pm}^{\mathrm{D}} = \frac{1}{2(\Gamma_+ + \tau_0^{\mathrm{sr}}\tau_1^{\mathrm{sr}}\lambda_l^{\mathrm{D}})}\left[(\tau_0^{\mathrm{sr}} + \tau_1^{\mathrm{sr}})\lambda_l^{\mathrm{D}} + 1 \pm \sqrt{\Delta}\right], \tag{C1}$$

$$A_{l\pm} = \frac{\Gamma_+}{2(\Gamma_+ + \tau_0^{\mathrm{sr}}\tau_1^{\mathrm{sr}}\lambda_l^{\mathrm{D}})}\left[1 \pm \frac{(\Gamma_-/\Gamma_+)(\tau_1^{\mathrm{sr}} - \tau_0^{\mathrm{sr}})\lambda_l^{\mathrm{D}} - 1}{\sqrt{\Delta}}\right], \tag{C2}$$

where

$$\Delta = \left[(\tau_1^{\mathrm{sr}} - \tau_0^{\mathrm{sr}})\lambda_l^{\mathrm{D}} + 1\right]^2 - 4(\eta_0/\eta_{\mathrm{z}})(\tau_1^{\mathrm{sr}} - \tau_0^{\mathrm{sr}})\lambda_l^{\mathrm{D}}, \tag{C3}$$

$$\Gamma_\pm = (\eta_0/\eta_{\mathrm{z}})\tau_1^{\mathrm{sr}} \pm (\eta_1/\eta_{\mathrm{z}})\tau_0^{\mathrm{sr}}. \tag{C4}$$

Note that

$$A_{l+} + A_{l-} = \frac{\Gamma_+}{(\Gamma_+ + \tau_0^{\mathrm{sr}}\tau_1^{\mathrm{sr}}\lambda_l^{\mathrm{D}})}, \tag{C5}$$

which is less than 1. So here also there is a missing amplitude, due to the fact that $\hat{G}(\infty) = 0$ for the Burgers model.

APPENDIX D: EFFECT OF INITIAL DEFORMED SHAPE

Both Fig. 2 and Eqs. (73a, b) make it clear that the precise shape of the initial deformation affects the recovery dynamics. In particular, an ellipsoid can be approximated well by a combination of the second- and fourth-order Legendre polynomials, as illustrated in Fig. 6(a) for an ellipsoid with a half-length $L = 1.4R$. [Note that, once L is specified, the half-width is fixed because of volume conservation.] In this case the P2 and P4 amplitudes determined by the best fit to the ellipsoid is 0.3206 and 0.0794, respectively. Recovery dynamics from such an initial ellipsoidal shape can be described by a corresponding linear combination of $f_2(t)$ and $f_4(t)$, leading to a bi-exponential decay [Fig. 6(b)].

REFERENCES

[1] A. Hubstenberger, S. L. Noble, C. Cameron, and T. C. Evans, *Translation Repressors, an RNA Helicase, and Developmental Cues Control RNP Phase Transitions During Early Development*, Dev Cell **27**, 161 (2013).

[2] S. Alberti and D. Dormann, *Liquid-Liquid Phase Separation in Disease*, Annu Rev Genet **53**, 171 (2019).

[3] S. Alberti, A. Gladfelter, and T. Mittag, *Considerations and Challenges in Studying Liquid-Liquid Phase Separation and Biomolecular Condensates*, Cell **176**, 419 (2019).

[4] W. Li, J. Hu, B. Shi, F. Palomba, M. A. Digman, E. Gratton, and H. Jiang, *Biophysical Properties of AKAP95 Protein Condensates Regulate Splicing and Tumorigenesis*, Nat Cell Biol **22**, 960 (2020).

[5] C. Roden and A. S. Gladfelter, *RNA Contributions to the Form and Function of Biomolecular Condensates*, Nat Rev Mol Cell Biol (2020).

[6] H. Yu *et al.*, *HSP70 Chaperones RNA-free TDP-43 Into Anisotropic Intranuclear Liquid Spherical Shells*, Science, eabb4309 (2020).

[7] A. Yamasaki, J. M. Alam, D. Noshiro, E. Hirata, Y. Fujioka, K. Suzuki, Y. Ohsumi, and N. N. Noda, *Liquidity Is a Critical Determinant for Selective Autophagy of Protein Condensates*, Mol Cell **77**, 1163 (2020).

[8] A. Patel *et al.*, *A Liquid-to-Solid Phase Transition of the ALS Protein FUS Accelerated by Disease Mutation*, Cell **162**, 1066 (2015).

[9] J. B. Woodruff, A. A. Hyman, and E. Boke, *Organization and Function of Non-dynamic Biomolecular Condensates*, Trends Biochem Sci **43**, 81 (2018).

[10] Z. Feng, X. Chen, X. Wu, and M. Zhang, *Formation of Biological Condensates via Phase Separation: Characteristics, Analytical Methods, and Physiological Implications*, J Biol Chem **294**, 14823 (2019).

[11] X. Gui *et al.*, *Structural Basis for Reversible Amyloids of hnRNPA1 Elucidates Their Role in Stress Granule Assembly*, Nat Commun **10**, 2006 (2019).

[12] L. Jawerth *et al.*, *Protein Condensates as Aging Maxwell Fluids*, Science **370**, 1317 (2020).

[13] H. Zhang, *The Glassiness of Hardening Protein Droplets*, Science **370**, 1271 (2020).

[14] C. P. Brangwynne, C. R. Eckmann, D. S. Courson, A. Rybarska, C. Hoege, J. Gharakhani, F. Julicher, and A. A. Hyman, *Germline P Pranules Are Liquid Droplets That Localize by Controlled Dissolution/Condensation*, Science **324**, 1729 (2009).

[15] C. P. Brangwynne, T. J. Mitchison, and A. A. Hyman, *Active Liquid-like Behavior of Nucleoli Determines Their Size and Shape in Xenopus laevis Oocytes*, Proc Natl Acad Sci U S A **108**, 4334 (2011).

[16] S. Elbaum-Garfinkle, Y. Kim, K. Szczepaniak, C. C. Chen, C. R. Eckmann, S. Myong, and C. P. Brangwynne, *The Disordered P Granule Protein LAF-1 Drives Phase Separation Into Droplets with Tunable Ciscosity and Dynamics*, Proc Natl Acad Sci U S A **112**, 7189 (2015).

[17] M. Feric, N. Vaidya, T. S. Harmon, D. M. Mitrea, L. Zhu, T. M. Richardson, R. W. Kriwacki, R. V. Pappu, and C. P. Brangwynne, *Coexisting Liquid Phases Underlie Nucleolar Subcompartments*, Cell **165**, 1686 (2016).

[18] H. Zhang, S. Elbaum-Garfinkle, E. M. Langdon, N. Taylor, P. Occhipinti, A. A. Bridges, C. P. Brangwynne, and A. S. Gladfelter, *RNA Controls PolyQ Protein Phase Transitions*, Mol Cell **60**, 220 (2015).

[19] L. M. Jawerth, M. Ijavi, M. Ruer, S. Saha, M. Jahnel, A. A. Hyman, F. Julicher, and E. Fischer-Friedrich, *Salt-Dependent Rheology and Surface Tension of Protein Condensates Using Optical Traps*, Phys Rev Lett **121**, 258101 (2018).

[20] H. X. Zhou, *Determination of Condensate Material Properties from Droplet Deformation*, J Phys Chem B **124**, 8372 (2020).

[21] H. X. Zhou, *Viscoelasticity of Biomolecular Condensates Conforms to the Jeffreys Model*, J Chem Phys, in press (2021).

[22] C. M. Caragine, S. C. Haley, and A. Zidovska, *Surface Fluctuations and Coalescence of Nucleolar Droplets in the Human Cell Nucleus*, Phys Rev Lett **121**, 148101 (2018).

[23] J. Wang *et al.*, *A Molecular Grammar Governing the Driving Forces for Phase Separation of Prion-like RNA Binding Proteins*, Cell **174**, 688 (2018).

[24] I. Alshareedah, T. Kaur, J. Ngo, H. Seppala, L. D. Kounatse, W. Wang, M. M. Moosa, and P. R. Banerjee, *Interplay between Short-Range Attraction and Long-Range Repulsion*

Controls Reentrant Liquid Condensation of Ribonucleoprotein-RNA Complexes, J Am Chem Soc **141**, 14593 (2019).

[25] S. Boeynaems *et al.*, *Spontaneous Driving Forces Give Rise to Protein-RNA Condensates with Coexisting Phases and Complex Material Properties*, Proc Natl Acad Sci U S A **116**, 7889 (2019).

[26] A. Ghosh and H. X. Zhou, *Determinants for Fusion Speed of Biomolecular Droplets*, Angew Chem Int Ed **59**, 20837 (2020).

[27] A. Prosperetti, *Viscous Effects on Perturbed Spherical Flows*, Q Appl Math **34**, 339 (1977).

[28] A. Prosperetti, *Free Oscillations of Drops and Bubbles: the Initial-Value Problem*, J Fluid Mech **100**, 333 (1980).

[29] W. Yu, M. Bousmina, C. Zhou, and C. L. Tucker III, *Theory for Drop Deformation in Viscoelastic Systems*, J Rheol **48**, 417 (2004).

[30] M. Minale, *Models for the Deformation of a Single Ellipsoidal Drop: a Review*, Rheol Acta **49**, 789 (2010).

[31] R. W. Hooper, V. F. de Almeida, C. W. Macosko, and J. J. Derby, *Transient Polymeric Drop Extension and Retraction in Uniaxial Extensional Flows*, J Nonnewton Fluid Mech **98**, 141 (2001).

[32] S. Mukherjee and K. Sarkar, *Effects of Viscoelasticity on the Retraction of a Sheared Drop*, J Nonnewton Fluid Mech **165**, 340 (2010).

[33] K. Verhulst, R. Cardinaels, P. Moldenaers, Y. Renardy, and S. Afkhami, *Influence of Viscoelasticity on Drop Deformation and Orientation in Shear Flow: Part 1. Stationary States*, J Nonnewton Fluid Mech **156**, 29 (2009).

[34] A. Luciani, M. F. Champagne, and L. A. Utracki, *Interfacial Tension Coefficient from the Retraction of Ellipsoidal Drops*, J Polym Sci B Polym Phys **35**, 1393 (1997).

[35] D. C. Tretheway and L. G. Leal, *Deformation and Relaxation of Newtonian Drops in Planar Extensional Flows of a Boger Fluid*, J Nonnewton Fluid Mech **99**, 81 (2001).

[36] K. Verhulst, R. Cardinaels, P. Moldenaers, S. Afkhami, and Y. Renardy, *Influence of Viscoelasticity on Drop Deformation and Orientation in Shear Flow. Part 2: Dynamics*, J Nonnewton Fluid Mech **156**, 44 (2009).

[37] S. Ali and V. M. Prabhu, *Characterization of the Ultralow Interfacial Tension in Liquid-Liquid Phase Separated Polyelectrolyte Complex Coacervates by the Deformed Drop Retraction Method*, Macromolecules **52**, 7495 (2019).

[38] S. Chandrasekhar, *Hydrodynamic and Hydromagnetic Stability* (CIarendon Press, Oxford, 1961).

[39] W. H. Reid, *The Oscillations of a Viscous Liquid Drop*, Q Appl Math **18**, 86 (1960).

[40] D. B. Khismatullin and A. Nadim, *Shape Oscillations of a Viscoelastic Drop*, Physical Review E **63**, 061508 (2001).

[41] G. Brenn and S. Teichtmeister, *Linear Shape Oscillations and Polymeric Time Scales of Viscoelastic Drops*, J Fluid Mech **733**, 504 (2013).

[42] L. G. Leal, *Advanced Transport Phenomena: Fluid Mechanics and Convective Transport Processes* (Cambridge University Press, Cambridge, 2007), Cambridge Series In Chemical Engineering.

[43] K. Akkaoui, M. Yang, Z. A. Digby, and J. B. Schlenoff, *Ultraviscosity in Entangled Polyelectrolyte Complexes and Coacervates*, Macromolecules **53**, 4234 (2020).

[44] Z. Benayad, S. von Bulow, L. S. Stelzl, and G. Hummer, *Simulation of FUS Protein Condensates with an Adapted Coarse-Grained Model*, J Chem Theory Comput **17**, 525 (2021).

[45] H. Stehfest, *Algorithm 368: Numerical Inversion of Laplace Transforms [D5]*, Commun ACM **13**, 47 (1970).

FIGURE CAPTIONS

FIG. 1. Illustration of the shape recovery of a deformed droplet. Left: initial deformation; right: fully recovered spherical shape.

FIG. 2. Comparison of droplet fusion dynamics and shape recovery dynamics. Fusion starts with two equal-sized droplets at contact and ends with a single larger spherical droplet having the same total volume. Deformation recovery is illustrated in Fig. 1; P2 and P4 indicate that the deformation is represented by the second- or fourth-order Legendre polynomial. L denotes the half-length of each system.

FIG. 3. Effect of the η_0/η_1 ratio on the shape recovery dynamics of viscoelastic droplets in an ideal fluid. The shear relaxation rate is fixed at $\tau_1^{\mathrm{sr}}\lambda_l^{\mathrm{D}} = 1$, where the two decay components of $f_l(t)$ have equal amplitudes. The values of η_0/η_1 are shown in the legend. The result for a Newtonian droplet is displayed for reference. The results in the figure are valid for any l.

FIG. 4. Effect of the shear relaxation rate on the shape recovery dynamics of viscoelastic droplets in an ideal fluid. The η_0/η_1 ratio is fixed at 1:5, whereas the values of $\tau_1^{\mathrm{sr}}\lambda_l^{\mathrm{D}}$ are shown in the legend. The result for a Newtonian droplet is displayed for reference. The results in the figure are valid for any l.

FIG. 5. Shape recovery curves at a finite viscosity ratio between the droplet and bulk phases. (a) Comparison of $f_2(t)$ for three cases of pairing interior and exterior fluids: Newtonian with Newtonian (solid curves), viscoelastic with Newtonian (dotted curves), and Newtonian with viscoelastic (dashed curves). The viscosity ratios, i.e. $\eta_{\mathrm{II}}/\eta_{\mathrm{I}}$, are shown in the legend. Viscoelasticity is given by the Jeffreys model, with η_0/η_1 = 1:5 and $\tau_1^{\mathrm{sr}}\gamma/\eta_{\mathrm{I}}R$ = 10. (b) Comparison of our analytical results (curves) with Verhulst et al.'s experimental data (symbols) for three systems, all with $\eta_{\mathrm{II}}/\eta_{\mathrm{I}}$ = 1.5. The viscoelasticity was reported as fitting to the Oldroyd B model, with $\eta_0/\eta_1 \approx$ 2:1 and $\tau_1^{\mathrm{sr}}\gamma/\eta_{\mathrm{I}}R$ indicated in the legend. Curves and symbols are matched in color for the same conditions.

FIG. 6. Effect of deformation shape on recovery dynamics. (a) Fit of an ellipsoid shape by a combination of the second- (P2) and fourth-order (P4) polynomials. The amplitudes of P2 and P4 are 0.3206R and 0.0794R, respectively, leading to a total half-length of 1.4R. (b) Comparison of the deformation decays curves for P2, P4, and their linear combination ("P2 + P4") that best fits the ellipsoid in panel (a). The dotted curve labelled "Exponential" displays the P2 component in the P2 + P4 curve. Inset: difference between the P2 + P4 curve and the P2 component at short times. The ordinate is in linear scale, in contrast to the log scale in the main figure.

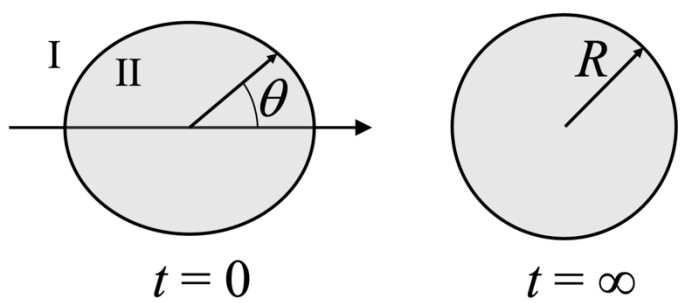

Figure 1

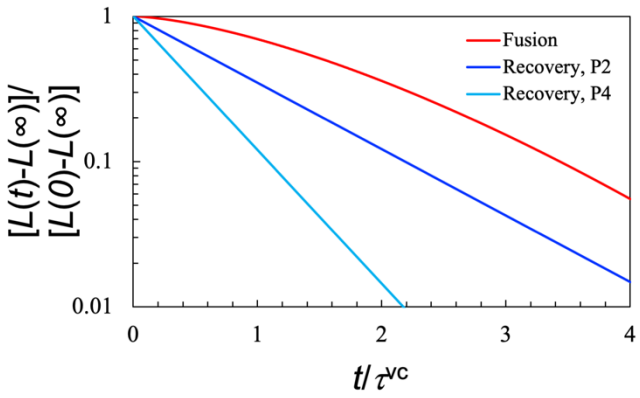

Figure 2

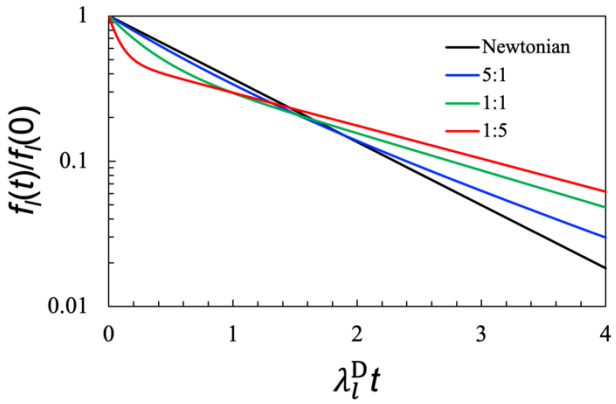

Figure 3

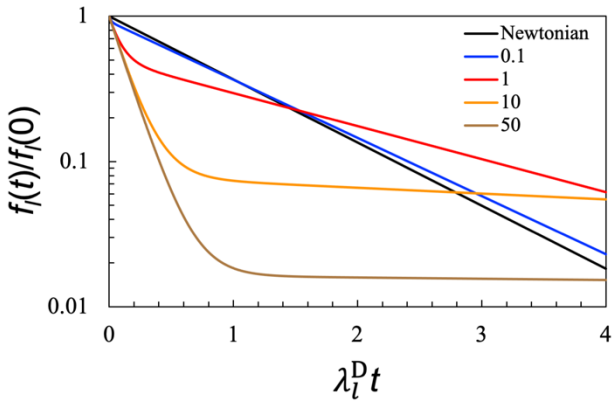

Figure 4

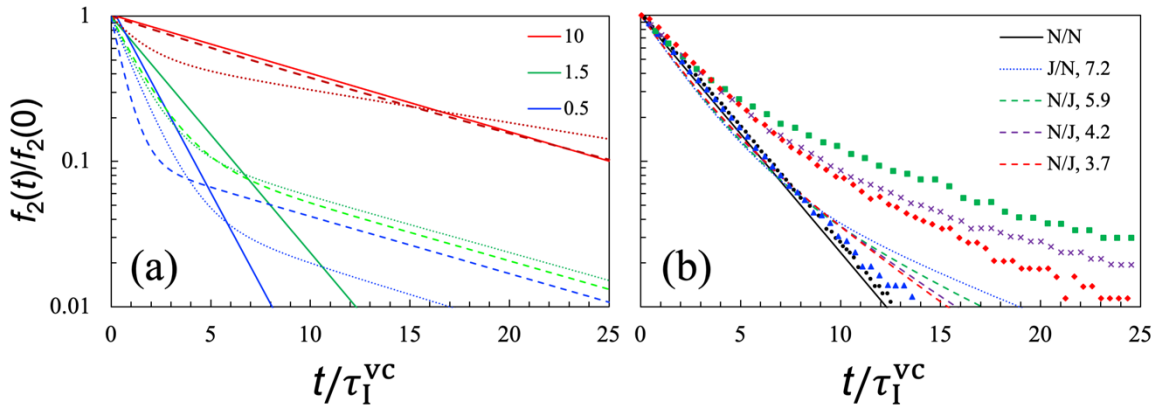
1
0.1
0.01
$f_2(t)/f_2(0)$
(a)
10
1.5
0.5
0
5
10
15
20
25
t/τ_I^{vc}
(b)
N/N
J/N, 7.2
N/J, 5.9
N/J, 4.2
N/J, 3.7
0
5
10
15
20
25
t/τ_I^{vc}

Figure 5

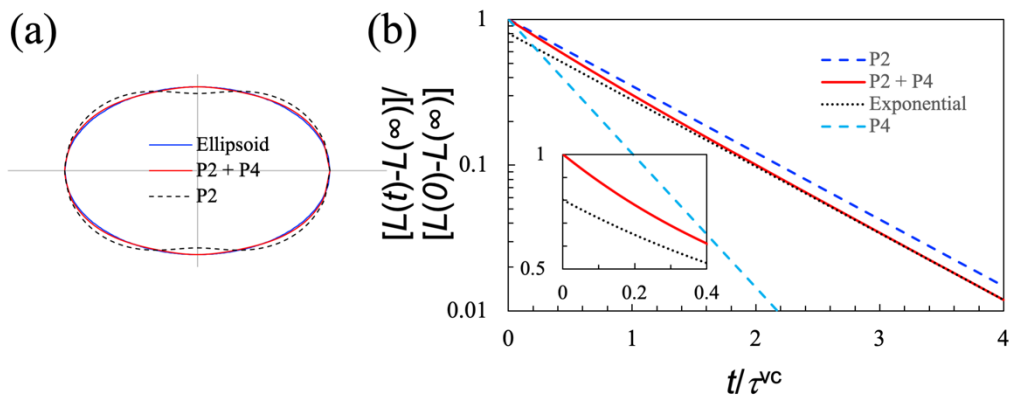
(a)
Ellipsoid
P2 + P4
P2
(b)
P2
P2 + P4
Exponential
P4
1
0.1
0.01
0
1
2
3
4
0.5
0.2
0.4
t/ τ^VC

Figure 6